Hydrogen atom in the presence of uniform magnetic and quadrupolar electric fields: Integrability, bifurcations, and chaotic behavior

M. Iñarrea and J. P. Salas
Area de Física Aplicada, Universidad de La Rioja, Edificio Científico Tecnológico, C/Madre de Dios 51, 26006 Logroño, Spain

V. Lanchares
Departamento de Matemáticas, Universidad de La Rioja, Edificio J. L. Vives, C/Luis de Ulloa, s/n, 26004 Logroño, Spain

(Received 12 July 2002; published 26 November 2002)

We investigate the classical dynamics of a hydrogen atom in the presence of uniform magnetic and quadrupolar electric fields. After some reductions, the system is described by a two degree of freedom Hamiltonian depending on two parameters. On the one hand, it depends on the z component of the canonical angular momentum P_ϕ, which is an integral because the system is axially symmetric; and on the other it also depends on a parameter representing the relative field strengths. We note that this Hamiltonian is closely related to the one describing the generalized van der Waals interaction. We report three cases of integrability. The structure and evolution of the phase space are explored intensively by means of Poincaré surfaces of section when the parameters vary. In this sense, we find several bifurcations that strongly change the phase space structure. The chaotic behavior of the system is studied and three order-chaos transitions are found when the system passes through the integrable cases. Finally, the ionization mechanics is studied.

DOI: 10.1103/PhysRevE.66.056614 PACS number(s): 05.45.−a, 39.10.+j, 52.25.Gj

I. INTRODUCTION

The hydrogen atom is a real integrable system. However, its integrability is frequently lost when the atom is subjected to external fields. The most famous example of this fact is the so-called Zeeman effect [1], when the applied field is a static magnetic field. In addition to the Zeeman effect, some more external perturbations have been added. Among them, we can cite the constant electric field (the Stark effect) [2], the microwave electric field [3], and the parallel [4] or crossed [5] electric and magnetic fields. These systems have been, during recent decades, unique laboratories where such aspects as the integrability and the quantum signatures of classical chaotic dynamics have been investigated [6]. In relation to the integrability, Alhassid *et al.* [7] introduced a general perturbation called the generalized van der Waals potential in which most of the cited static perturbations are represented. In atomic units and cylindrical coordinates $(\rho,z,\phi,P_\rho,P_z,P_\phi)$, the Hamiltonian of a hydrogen atom perturbed by a generalized van der Waals potential can be written as

$$\mathcal{H}=\frac{P_\rho^2+P_z^2}{2}+\frac{P_\phi^2}{2\rho^2}-\frac{1}{\sqrt{\rho^2+z^2}}+\frac{\alpha}{2}(\rho^2+\beta^2 z^2). \quad (1)$$

Owing to the axial z symmetry, the z component P_ϕ of the canonical angular momentum is conserved and this Hamiltonian defines a two degree of freedom dynamical system. For $\beta=0$ the Hamiltonian (1) is that of the hydrogen atom in a constant magnetic field (the quadratic Zeeman effect), for $\beta=\pm 1$ it is the spherical quadratic Zeeman effect, and when $\beta=\pm\sqrt{2}$ the Hamiltonian (1) describes the instantaneous van der Waals interaction between the atom and a metal surface [8].

One of the most important results of the study of this system is that the problem is shown to be integrable for the special values $\beta=\pm 1/2,\pm 1,\pm 2$ [9–11]. In this sense, for these values of β additional constants of the motion have been found [9–12]. However, while for $\beta=\pm 1,\pm 2$ the system is separable, respectively, into spherical and parabolic coordinates, for $\beta=\pm 1/2$ the system seems to be one of the rare cases of an integrable but nonseparable system [12]. It is also worth noticing that when the sign of the Coulomb term is changed, the resulting Hamiltonian represents the motion of two ions in a Paul trap [13,14], and the cited integrable limits also hold in this case. Finally, a semiclassical approach [15] and the quantum manifestation of chaos [16] in this system have been investigated by Ganesan and Lakshmanan. More recently, Beims and Gallas [17] introduced a more general system that includes the presence of a static electric field, in such a way that two more cases of integrability are reported.

At this point, the aim of this paper is to follow the idea of Blümel and Reinhardt [18] that a general β value in Eq. (1) would correspond to a hydrogen atom in the presence of a constant magnetic field and a quadrupolar electric field. However, as we will see, this field configuration is not completely described by the Hamiltonian (1), but by a slightly different one. Moreover, we emphasize that, while the system (1) can be used just as a theoretical toy, the system that we present in this work may be tested in the laboratory because, nowadays, almost perfect quadrupolar electric fields are implemented, for example, in ion Penning traps. We leave a more deeper discussion about this important and complex question to experimentalists.

The paper is organized as follows. Section II is devoted to the posing of the problem. We show that the problem has two degrees of freedom and it depends on two parameters. The shape of the effective potential surface and its critical points are studied depending on the system parameters. In Sec. III

 ©2002 The American Physical Society

we analyze the three integrable cases of the problem. By means of Levi-Civitá regularizations, we study the separability of the Hamiltonian system and find the global invariant (integrals) of the problem in those cases. In Sec. IV we study the evolution of the phase space structure as the parameters vary, and several bifurcations are found. In Sec. V we analyze the chaotic behavior and the ionization mechanics of the system. Finally, in Sec. VI the main results of the paper are summarized.

II. THE PROBLEM

Let us consider the motion of an electron of mass m and charge $-q$ in a Coulomb field induced by an infinitely massive nucleus of charge $q>0$ at rest. On the central field, a uniform constant magnetic field $\boldsymbol{B}=B\hat{\mathbf{z}}$ and a quadrupolar electric potential given by

$$V_Q=m\frac{w_z^2}{4}(2z^2-x^2-y^2)$$

are superimposed.

As we noted in the Introduction, this field arrangement is also used in ion Pennig traps, in such a way that w_z is the axial frequency induced by the quadrupole electric field. As well as the dependence on the charge $-q$ and on the mass m of the electron, this frequency depends on the experimental configuration of the electrodes that create the quadrupolar electric potential [19,20].

In cylindrical coordinates $(\rho,z,\phi,P_\rho,P_z,P_\phi)$ and atomic units $(m=q=1)$, it is quite simple to see that the classical Hamiltonian of the system is given by

$$\mathcal{H}=\frac{P_\rho^2+P_z^2}{2}+\frac{P_\phi^2}{2\rho^2}-\frac{1}{\sqrt{\rho^2+z^2}}-\gamma P_\phi+\frac{\gamma^2}{2}\rho^2+\frac{w^2}{2}\left(z^2-\frac{\rho^2}{2}\right), \tag{2}$$

where $\gamma=B/2B_0$ and $w=w_z/w_0$ are, respectively, the reduced Larmor frequency ($B_0\approx 2.35\times 10^5$ T) and the reduced axial frequency ($w_0\approx 2.067\times 10^{16}$ s^{-1}).

Due to the axial symmetry, a time dependent canonical transformation allows us to formulate the problem in a frame of reference rotating with angular velocity γ. In this moving frame the paramagnetic term γP_ϕ is not present, and the Hamiltonian of the system is

$$\mathcal{H}=\frac{P_\rho^2+P_z^2}{2}+\frac{P_\phi^2}{2\rho^2}-\frac{1}{\sqrt{\rho^2+z^2}}+\frac{\gamma^2}{2}\rho^2+\frac{w^2}{2}\left(z^2-\frac{\rho^2}{2}\right). \tag{3}$$

This Hamiltonian depends on the four parameters γ, α, P_ϕ, and the energy $E=\mathcal{H}$. Following several authors [1], we can scale the coordinates $\boldsymbol{r}=(\rho,z)$ and momenta $\boldsymbol{P}=(P_\rho,P_z,P_\phi)$ as

$$\boldsymbol{r}'=\gamma^{2/3}\boldsymbol{r},\quad \boldsymbol{P}'=\gamma^{-1/3}\boldsymbol{P},$$

in such a way that, after dropping th primes in coordinates and momenta, the Hamiltonian (3) becomes

$$\mathcal{H}'=\frac{\mathcal{H}}{\gamma^{2/3}}=\epsilon=\frac{P_\rho^2+P_z^2}{2}+\frac{P_\phi^2}{2\rho^2}-\frac{1}{\sqrt{\rho^2+z^2}}+\frac{1}{2}\left(1-\frac{\lambda^2}{2}\right)\rho^2+\frac{\lambda^2}{2}z^2, \tag{4}$$

where the new dimensionless parameter $\lambda=w/\gamma$ represents the ratio between the strengths of the two external fields. Hence, the classical dynamics of the system does not depend on those four parameters independently but only on λ, P_ϕ, and the new scaled energy $\epsilon=E\gamma^{-2/3}$.

Note that when $\lambda<\sqrt{2}$ we can define the parameters α and β as

$$\alpha=1-\frac{\lambda^2}{2},\quad \beta=\sqrt{\frac{2\lambda^2 4}{2-\lambda^2}}, \tag{5}$$

and the system (4) is equivalent to the Hamiltonian (1). However, the case $\lambda>\sqrt{2}$ is not included in the generalized van der Waals model (1), and hence we will use the Hamiltonian (4), because it represents the correct model to study the considered system.

The effective potential

In order to see how the external fields modify the dynamics of the atom we have applied the common and useful method of studying the shape of the effective potential $U(\rho,z)$ in Eq. (4),

$$U(\rho,z)=\frac{P_\phi^2}{2\rho^2}-\frac{1}{\sqrt{\rho^2+z^2}}+\frac{1}{2}\left(1-\frac{\lambda^2}{2}\right)\rho^2+\frac{\lambda^2}{2}z^2, \tag{6}$$

as the parameters P_ϕ and λ vary. The critical points of $U(\rho,z)$ as a function of the parameters P_ϕ and λ are given by the solutions of the equations

$$\frac{\partial U}{\partial\rho}=U_\rho=-\frac{P_\phi^2}{\rho^3}+\frac{\rho}{(\rho^2+z^2)^{3/2}}+\left(1-\frac{\lambda^2}{2}\right)\rho=0, \tag{7}$$

$$\frac{\partial U}{\partial z}=U_z=z\left[\frac{1}{(\rho^2+z^2)^{3/2}}+\lambda^2\right]=0. \tag{8}$$

From Eq. (8) it follows that the critical points lie on the plane $z=0$. After introducing $z=0$ in Eq. (7), we get

$$U_\rho(\rho,z=0)=-\frac{P_\phi^2}{\rho^3}+\frac{1}{\rho^2}+\left(1-\frac{\lambda^2}{2}\right)\rho=0, \tag{9}$$

which gives rise to the following polynomial equation in ρ:

$$\mathcal{P}\equiv\left(1-\frac{\lambda^2}{2}\right)\rho^4+\rho-P_\phi^2=0. \tag{10}$$

The right hand side of Eq. (10), $\mathcal{P}$, is a fourth degree polynomial in ρ whose positive roots give the ρ coordinate of the critical points. Although there is a general formula giving the roots of $\mathcal{P}$ in exact terms, we are more interested in knowing their number, nature, and conditions of existence.

In order to know the number of positive roots of $\mathcal{P}$, we use the criterion of Descartes [21]. The rule of Descartes establishes that, if p is the number of positive roots and s is the number of sign changes in the coefficient sequence of a polynomial, then $s=p+2k$, where k is a positive integer. By virtue of this theorem, from the changes of sign in the sequence of coefficients of $\mathcal{P}$, we deduce that (1) for $\lambda<\sqrt{2}$, the polynomial $\mathcal{P}$ presents one change of sign, and thus it has one root; (2) for $\lambda>\sqrt{2}$, the polynomial $\mathcal{P}$ presents two changes of sign, and thus it has two or zero roots.

For $P_\phi=0$, we can easily solve Eq. (10), in such a way that we find two solutions

$$\rho_0=0,\quad \rho_1=\left(\frac{2}{\lambda^2-2}\right)^{1/3}. \tag{11}$$

Note that the first solution does not correspond to any critical point because neither Eq. (7) nor Eq. (8) is satisfied. In fact, they are not defined at $z=0$, $\rho=0$. However, for $P_\phi\neq0$, by means of the implicit function theorem, we find a root of Eq. (10) $\rho_0(P_\phi)$ which is no longer zero unless $P_\phi=0$. Then we obtain a proper critical point of coordinates $(\rho_0,0)$, that is the unique critical point for $\lambda<\sqrt{2}$. On the other hand, the second solution ρ_1 only has sense for $\lambda>\sqrt{2}$ and hence in this case the number of critical points must be 2 instead of zero, namely, ρ_0,ρ_1.

To know the type of critical point at hand, we calculate the determinant ΔH of the Hessian matrix H,

$$\Delta H=\det H,\quad H=\begin{pmatrix}U_{\rho\rho} & U_{\rho z}\\ U_{\rho z} & U_{zz}\end{pmatrix}. \tag{12}$$

For $z=0$, the elements of H are

$$U_{\rho z}=0,$$

$$U_{\rho\rho}=\frac{3P_\phi^2}{\rho^4}-\frac{2}{\rho^3}+1-\frac{\lambda^2}{2},$$

$$U_{zz}=\lambda^2+\frac{1}{\rho^3}. \tag{13}$$

Because U_{zz} is a positive term, the nature of the critical points is determined by the sign of the element $U_{\rho\rho}$. For $P_\phi=0$, we focus on the nature of $(\rho_1,0)$. By substitution in $U_{\rho\rho}$, we get that

$$U_{\rho\rho}(P_2)=3\left(1-\frac{\lambda^2}{2}\right)<0,$$

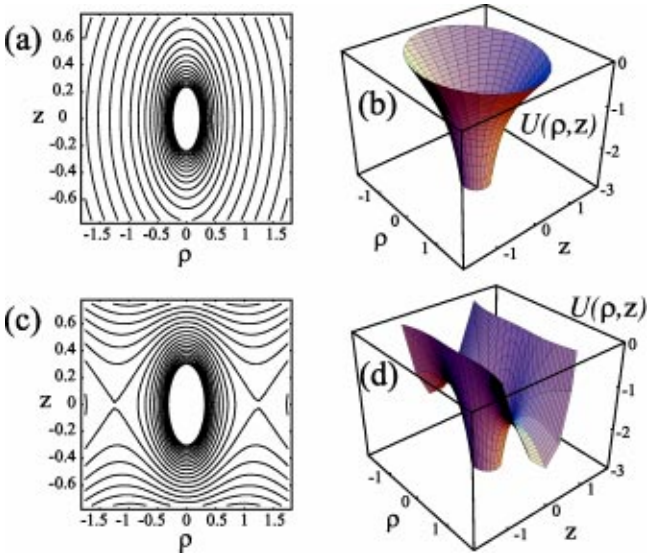

FIG. 1. Equipotential curves of $U(\rho,z)$ and potential energy surfaces $U(\rho,z)$ for $P_\phi=0$, (a) and (b) $\lambda=1$, (c) and (d) $\lambda=2$.

because $\lambda>\sqrt{2}$. Hence, $(\rho_1,0)$ is always a saddle point whose energy is E_2,

$$E_2=-\frac{3}{2}\left(\frac{\lambda^2-2}{2}\right)^{1/3}<0.$$

In Fig. 1 we show the potential energy surface $U(\rho,z)$ and its equipotential curves for $P_\phi=0$ and both cases $\lambda<\sqrt{2}$ and $\lambda>\sqrt{2}$. We have plotted these figures for positive and negative values of ρ because, although it is a cylindrical coordinate, in the case $P_\phi=0$, ρ can also be considered as a Cartesian coordinate with positive and negative values in the orbital plane, which is always perpendicular to the x-y plane [22].

For the general case $P_\phi\neq0$, the numerical resolution of Eq. (10) provides the same results, e.g., for $\lambda<\sqrt{2}$ the effective potential shows only a minimum, and for $\lambda>\sqrt{2}$ it shows a minimum and a saddle point. These situations are depicted in Fig. 2.

We can conclude that for $\lambda<\sqrt{2}$ the atom, even for positive energies, cannot ionize. However, for $\lambda>\sqrt{2}$ the electron has the possibility of escaping through the channel created by the saddle point. This question will be studied in Sec. V.

III. INTEGRABLE CASES

As we said, for $\lambda<\sqrt{2}$ the Hamiltonian (4) is formally equivalent to the Hamiltonian (1) describing the generalized van der Waals system. Hence, the integrable cases of Eq. (1) for $\beta_i=(\pm1/2,\pm1,\pm2)$ must have their counterparts when the integrability of Eq. (4) is considered. In this way, we obtain the corresponding values of λ_i by solving the equation

$$\beta^2=\frac{2\lambda^2}{2-\lambda^2} \tag{14}$$

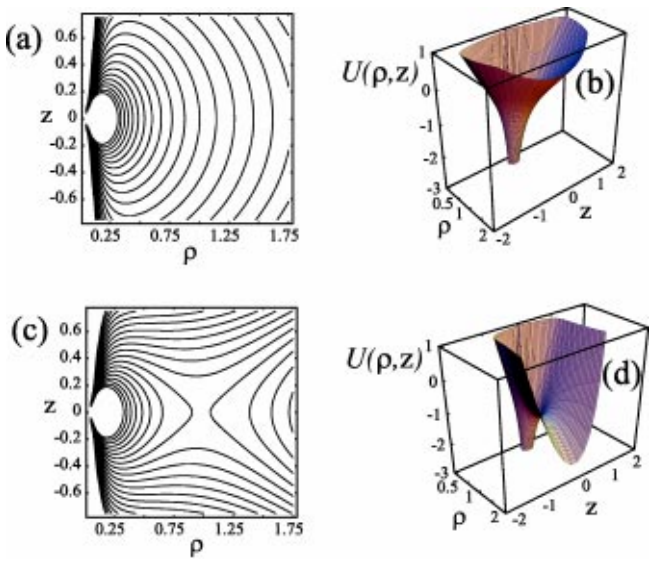

FIG. 2. Equipotential curves of $U(\rho,z)$ and potential energy surfaces $U(\rho,z)$ for $P_\phi=0.25$, (a) and (b) $\lambda=1$, (c) and (d) $\lambda=2$.

for $\beta_i=(\pm 1/2,\pm 1,\pm 2)$. We get, respectively, $\lambda_i=(\pm\sqrt{2}/3,\pm\sqrt{2/3},\pm 2/\sqrt{3})$. For each value β_i, the corresponding third constant of the motion of the system (1) was calculated for all α values and $P_\phi=0$ in [10] and for all P_ϕ and $\alpha=1$ in [12]. However, because in the Hamiltonian (4) the parameters α and β are both dependent on λ [see Eq. (5)] those three functions may not be the global invariants of Eq. (4) in the cases λ_i. Hence, we have determined the correct integrals $I(\rho,z)$ of Eq. (4) for λ_i. This study can be summarized as follows.

(1) For $\lambda=\pm\sqrt{2/3}$ and for all P_ϕ, the Hamiltonian (4) is separable in spherical coordinates and the problem is a one degree of freedom system depending on the radial distance. In this case, we find the same integral as for $\alpha=1$ and $\beta_i=\pm 1$,

$$I_1=(\rho P_z-zP_\rho)^2+\frac{P_\phi^2 z^2}{\rho^2}. \tag{15}$$

(2) When $\lambda=\pm 2/\sqrt{3}$ and for all P_ϕ, the Hamiltonian (4), like the Hamiltonian (1) for $\beta=\pm 2$ [12], is separable in semiparabolic coordinates (u,v),

$$\rho=uv,\quad z=(u^2-v^2)/2. \tag{16}$$

Expressed in those variables, the Hamiltonian (4) reads

$$\mathcal{K}=2=\frac{P_u^2+P_v^2}{2}+\frac{P_\phi^2}{2}\left(\frac{1}{u^2}+\frac{1}{v^2}\right)-\epsilon(u^2+v^2)+\frac{1}{2}\left(1-\frac{\lambda^2}{2}\right)(u^2+v^2)u^2v^2+\frac{1}{8}\lambda^2(u^2-v^2)^2(u^2+v^2), \tag{17}$$

where we have defined a new scaled time $\tau=t/(u^2+v^2)$ and multiplied by u^2+v^2. This procedure is the so-called Levi-Civitá regularization [23]. We observe that separability of Eq. (17) only takes place when $\lambda=\pm 2/\sqrt{3}$. For this λ value, the Hamiltonian $\mathcal{K}$ is

$$\mathcal{K}=2=\frac{P_u^2+P_v^2}{2}+\frac{P_\phi^2}{2}\left(\frac{1}{u^2}+\frac{1}{v^2}\right)-\epsilon(u^2+v^2)+\frac{u^6}{6}+\frac{v^6}{6}, \tag{18}$$

and its separability is clear. For this separable case, we find the following integral of motion in cylindrical coordinates:

$$I_2=-\frac{P_\phi^2 z}{\rho^2}+\frac{\rho^2 z}{3}+P_\rho(P_z\rho-P_\rho z)+\frac{z}{\sqrt{\rho^2+z^2}}. \tag{19}$$

Note that this invariant is different from that found for Eq. (1) when $\beta_i=\pm 2$ [12].

(3) For $\lambda=\pm\sqrt{2}/3$, as for the Hamiltonian (1) for $\beta_i=\pm 2$ [12], we find that the problem separates only for $P_\phi=0$ when a Levi-Civitá regularization is applied using the semiparabolic coordinates (u,v),

$$\rho=(u^2-v^2)/2,\quad z=uv. \tag{20}$$

Indeed, after the regularization, the Hamiltonian (4) results in

$$\mathcal{K}=2=\frac{P_u^2+P_v^2}{2}+\frac{P_\phi^2(u^2+v^2)}{(u^2-v^2)^2}-\epsilon(u^2+v^2)+\frac{1}{8}\left(1-\frac{\lambda^2}{2}\right)(u^2-v^2)^2(u^2+v^2)+\frac{\lambda^2}{2}u^2v^2(u^2+v^2). \tag{21}$$

And for $\lambda=\pm\sqrt{2}/3$, it takes the form

$$\mathcal{K}=2=\frac{P_u^2+P_v^2}{2}+\frac{P_\phi^2(u^2+v^2)}{(u^2-v^2)^2}-\epsilon(u^2+v^2)+\frac{u^6}{9}+\frac{v^6}{9}, \tag{22}$$

which separates only when $P_\phi=0$. However, for all P_ϕ we find the following invariant:

$$I_3=\frac{9P_\phi^2(P_\rho\rho+P_z z)^2}{8\rho^2}+P_\phi^2(\rho^2+z^2)+\left(\frac{3P_\phi^2}{2\sqrt{2}\rho}-\frac{\rho z^2}{3\sqrt{2}}+\frac{3P_z(P_z\rho-P_\rho z)}{2\sqrt{2}}-\frac{3\rho}{2\sqrt{2}\sqrt{\rho^2+z^2}}\right)^2. \tag{23}$$

Again, this invariant is different from that found in the generalized van der Waals problem when $\beta_i=\pm 1/2$ [12]. As

was pointed out by Farrelly and Uzer, this case is considered in the literature a rare example of an integrable but nonseparable system [12].

IV. PHASE SPACE STRUCTURE

In this section we are interested in the study of the phase space governed by the Hamiltonian (4). As is well known, the phase space structure is mainly characterized by the number and stability of the periodic orbits existing in phase space [24]. When dealing with a system of two degrees of freedom, the computation of surfaces of section allows us to illustrate the phase space structure: in the regions of the phase space where the motion is regular, periodic orbits are clearly identified as fixed points of the Poincaré map. With this technique, we explore the evolution of the phase space as the parameters $(\epsilon,\lambda,P_\phi)$ vary.

It is convenient to consider separately the cases $P_\phi=0$ and $P_\phi\neq 0$, because they require different formulations in order to carry out the corresponding Poincaré map.

A. Case $P_\phi=0$

When $P_\phi=0$, the orientation of the orbital plane (ρ,z) is always perpendicular to the x-y plane. We recall that, although ρ is a cylindrical coordinate, in the case $P_\phi=0$, it can be considered as a Cartesian coordinate in the orbital plane with positive and negative values, and normal to the z axis [22]. Moreover, because a centrifugal barrier is not present, the electron can reach the origin and it is more illustrative to work in coordinates $(\pm\rho,z)$. However, we have to take into account that when the electron reaches the origin $\boldsymbol{r}\rightarrow\mathbf{0}$, the Hamiltonian (4) presents a singularity. The common way to avoid the numerical problems involved with that singularity is to apply a Levi-Civitá regularization [23]. Because this procedure has already been applied twice to Eq. (4) in the previous section, we will use one of the resulting Hamiltonians. In particular, we will use the Hamiltonian (21).

For $P_\phi=0$, the Hamilton equations of motion arising from Eq. (21) are

$$\dot{u}=P_u,$$

$$\dot{P}_u=\frac{1}{8}u[16\epsilon+3(-2+d^2)u^4+2(2-9d^2)u^2v^2+(2-9d^2)v^4],$$

$$\dot{v}=P_v,$$

$$\dot{P}_v=\frac{1}{8}v[16\epsilon+(2-9d^2)u^4+2(2-9d^2)\times u^2v^2+3(-2+d^2)v^4]. \tag{24}$$

In searching for particular solutions of Eq. (24), we find the following.

(1) Rectilinear orbits along the u axis ($v=0$) always exist. These orbits correspond to rectilinear orbits along the positive ρ axis. In the literature, these orbits are named as I_1 [1].

(2) Rectilinear orbits along the v axis ($u=0$) always exist. These orbits, named I_1', correspond to rectilinear orbits along the negative ρ axis.

(3) Rectilinear orbits $v=\pm u$ always exist, and correspond to rectilinear orbits along the z axis. In the literature, these orbits are named I_∞ [1].

(4) Rectilinear orbits $v=au$ exist for all $a\neq(0,\pm1,\pm\infty)$ only when $\lambda=\sqrt{2/3}$. These orbits correspond to rectilinear orbits $z=[a/(1-a)]\rho$. Note that when these rectilinear orbits appear, the system is integrable.

To look for additional periodic orbits, we compute the surfaces of section by numerical integration of the equations of motion (24) by means of a Runge-Kutta algorithm of fifth order with fixed step [25]. We have defined the surface of section projecting the phase space on the $u=0$ plane with $P_u\geqslant 0$. Under these conditions, the available region on the surface of section is limited by the curves

$$P_v=\pm\sqrt{4+2\epsilon v^2-\left(1-\frac{\lambda^2}{2}\right)\frac{v^6}{4}}. \tag{25}$$

It is worth noting that the curves defined by Eq. (25) correspond to the rectilinear orbit I_1', as can be checked in Eq. (21). In order to study the evolution of the structure of the phase space, several surfaces of section were generated by keeping the scaled energy ϵ constant while varying the parameter λ.

We begin the study by revising the quadratic Zeeman effect case, $\lambda=0$. The corresponding surface of section is shown in Fig. 3(a). We take $\epsilon=-2$ because for this energy the system is still close to the integrable limit $\epsilon\rightarrow-\infty$ [1], and all orbits are regular and confined to adiabatic invariant tori. This surface of section shows four important structures.

(1) The stable (elliptic) fixed point located at (0,0) which corresponds to the rectilinear orbits I_1. The levels around this point are quasiperiodic orbits with the same symmetry pattern as I_1; that is to say, mainly localized along the u axis, e.g., along the positive ρ axis [see Fig. 3(b)].

(2) The two elliptic fixed points located at $(0,\pm\sqrt{2})$ which correspond to the rectilinear orbits I_∞. We can observe in Fig. 3(b) that orbits around these fixed points are quasiperiodic orbits mainly localized along the z axis.

(3) The two unstable (hyperbolic) fixed points of the separatrix which divides the previous regions of motion. These hyperbolic points, named C, correspond to almost circular orbits located at $(\pm1/\sqrt{-\epsilon},0)$. They become circular orbits when the energy $\epsilon\rightarrow-\infty$.

(4) Finally, and taking into account that the limit of the surface of section corresponds to the rectilinear orbit I_1' ($u=0$), the levels above the separatrix are quasiperiodic orbits mainly localized along the v axis, e.g., along the negative ρ axis [see Fig. 3(b)].

At this point, it is clear that the stability of I_1' cannot be determined by looking at the surface of section, because this

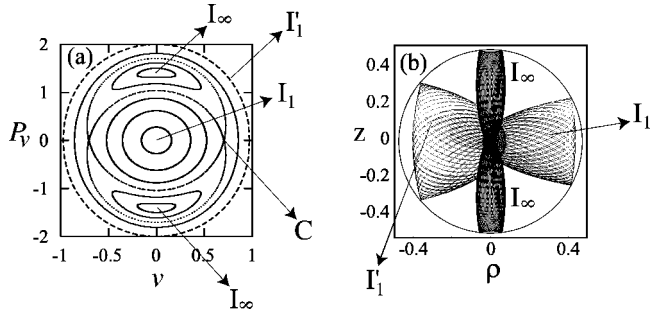

FIG. 3. (a) Surface of section ($u=0, P_u \geqslant 0$). (b) Quasiperiodic orbits around I_1, I_1', and I_∞. Both figures for $\epsilon=-2$, $P_\phi=0$, and $\lambda=0$

orbit does not appear as a single fixed point. However, we can determine its stability if we consider that the surface of section is homeomorphic to the quotient space obtained by identifying the points of the limit of the section [26]. Indeed, the domain D of the surface of section is defined in the plane (v, P_v) by the inequality

$$4+2\epsilon v^2-\left(1-\frac{\lambda^2}{2}\right)\frac{v^6}{4}-P_v^2 \geqslant 0,$$

the points of the border (25) being those that satisfy

$$\Gamma \equiv 4+2\epsilon v^2-\left(1-\frac{\lambda^2}{2}\right)\frac{v^6}{4}-P_v^2=0.$$

Now, we can define a continuous function that maps D onto the two-dimensional sphere $\mathcal{S}^2$ in such a way that the border Γ is mapped to the north pole of the sphere. Let $\xi(v, P_v)$ be a non-negative function defined as

$$\xi(v,P_v)=\sqrt{4+2\epsilon v^2-\left(1-\frac{\lambda^2}{2}\right)\frac{v^6}{4}-P_v^2}. \qquad (26)$$

This function, which acts as a radial distance on the domain D, varies from 0 to 2, and it takes the maximum value at (0,0) and the minimum value at the border Γ. Thus, the function defined as

$$f:\ D \to \mathcal{S}^2,$$

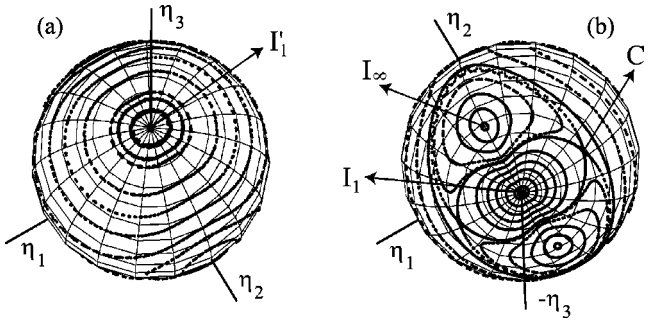

FIG. 4. Transformation of the surface of section ($u=0, P_u \geqslant 0$) onto the sphere $\mathcal{S}^2$, $\lambda=0$, $\epsilon=-2$, and $P_\phi=0$, (a) North view, (b) South view.

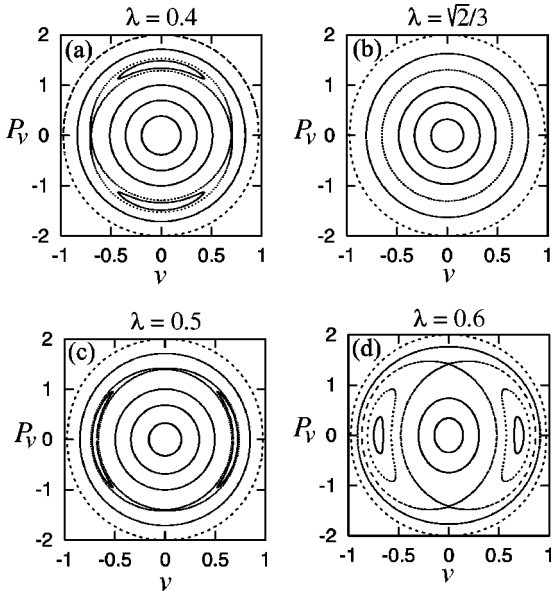

FIG. 5. Evolution of the surfaces of section ($u=0, P_u \geqslant 0$) as a function of λ for $\epsilon=-2$ and $P_\phi=0$. The first *oyster* bifurcation is observed between (a) and (c).

$$(x,P) \mapsto (\eta_1, \eta_2, \eta_3),$$

$$(v,P_v) \mapsto (\xi\cos\theta, \xi\sin\theta, \sqrt{1-\xi^2}) \quad \text{if} \quad 0 \leqslant \xi < 1,$$

$$(v,P_v) \mapsto ((2-\xi)\cos\theta, (2-\xi)\sin\theta, -\sqrt{1-(2-\xi)^2}) \quad \text{if} \quad 1 \leqslant \xi \leqslant 2, \qquad (27)$$

where

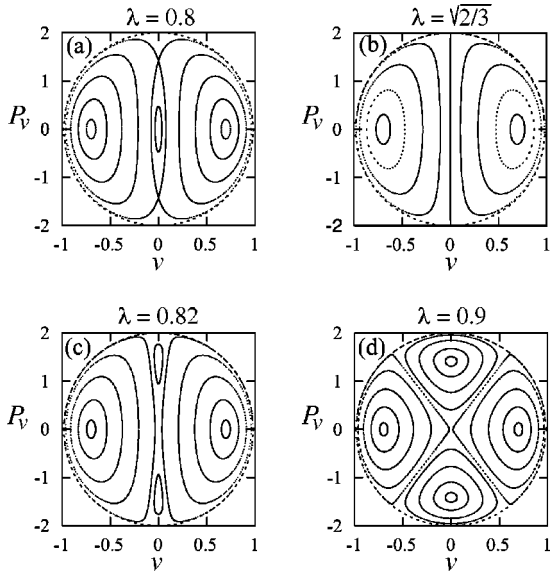

FIG. 6. Evolution of the surfaces of section ($u=0, P_u \geqslant 0$) as a function of λ for $\epsilon=-2$ and $P_\phi=0$. The second oyster bifurcation is observed between (a) and (c).

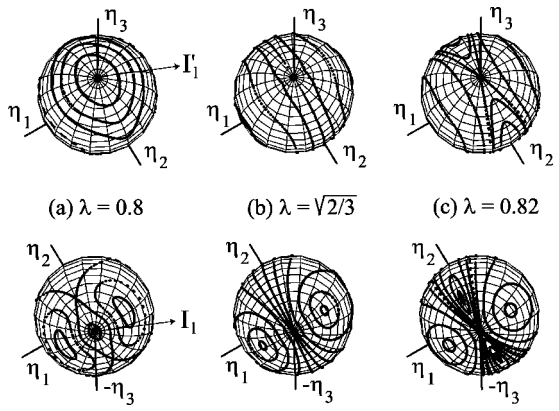

FIG. 7. Representation of the second oyster bifurcation on the sphere $\mathcal{S}^2$. Upper row, north view. Lower row, south view. $\epsilon = -2$ and $P_\phi = 0$.

$$\sin\theta = \frac{P_v}{\sqrt{v^2+P_v^2}}, \quad \cos\theta = \frac{v}{\sqrt{v^2+P_v^2}},$$

maps D onto the two-dimensional sphere $\mathcal{S}^2$ of unit radius,

$$\mathcal{S}^2 = \{(\eta_1,\eta_2,\eta_3)\,|\,\eta_1^2+\eta_2^2+\eta_3^2=1\},$$

where the border Γ is mapped to the north pole $(1,0,0)$. Moreover, those points satisfying $0<\xi<1$ are mapped to the southern hemisphere, and those satisfying $1\leqslant\xi\leqslant 2$ to the northern one.

The Euler characteristic of $\mathcal{S}^2$ is 2, and by virtue of the index theorem [27] the sum of the indexes of the critical points must be 2. Note that in our system the limit of the surface of section (v,P_v) is the periodic orbit I_1', and transforms to an equilibrium at $(1,0,0)$ in $\mathcal{S}^2$. Because the surface of section shows two unstable fixed points (with index -1) and three stable fixed points (with index 1), the fixed point I_1' at the north pole must be stable (with index 1). We can observe this fact in Fig. 4 which shows the result of applying the above transformation (27) to the surface of section of Fig. 3(a).

In general, when the domain D of the surface of section is defined in a certain plane (x,P) by the inequality

$$D \equiv g(x) - P^2 \geqslant 0,$$

we can construct a homeomorphism from D to the quotient space resulting from the identification of the points of the border

$$\Gamma \equiv g(x) - P^2 = 0.$$

In this case it is possible to extend the transformation (27), defining a two-dimensional function

$$\xi = \sqrt{g(x)-P^2},$$

which plays the role of a radius. It takes the minimum value 0 at the border Γ and the maximum value ξ_M at $(x_M,0)$. Now, the family of functions

$$\begin{aligned} &f_n:\ D \to \mathcal{S}^2, \\ &(x,P) \mapsto (\xi_1\cos\theta, \quad \xi_1\sin\theta, \quad \sqrt{1-\xi_1^2}) \\ &\text{if} \quad 0<\xi<x_M/n, \\ &(x,P) \mapsto (\xi_2\cos\theta, \quad \xi_2\sin\theta, \quad -\sqrt{1-\xi^2}) \\ &\text{if} \quad x_M/n<\xi<x_M, \end{aligned} \tag{28}$$

where $n \in \mathbf{N}$ and

$$\xi_1 = \frac{n\xi}{x_M}, \quad \xi_2 = \frac{n}{n-1}\left(1-\frac{\xi}{x_M}\right),$$

$$\sin\theta = \frac{P}{\sqrt{(x-x_M)^2+P^2}},$$

$$\cos\theta = \frac{x-x_M}{\sqrt{(x-x_M)^2+P^2}},$$

maps D onto the two-dimensional sphere $\mathcal{S}^2$ of unit radius

$$\mathcal{S}^2 = \{(\eta_1,\eta_2,\eta_3)\,|\,\eta_1^2+\eta_2^2+\eta_3^2=1\}.$$

Note that we can map on the northern or southern hemisphere the n fraction of the surface of section in terms of the radial function ξ. However, if the level contours of ξ in the domain D are not smoothly distributed ("concentric"), the transformation deforms the aspect of the Poincaré map, and more complicated transformations must be performed.

In fact, let us note that in order to know the stability of the periodic orbit represented by the limit of the surface of section, it is not necessary to perform the transformation. Taking into account that the Poincaré index of the sphere is 2 and that the limit of the surface of section is one of the critical points on $\mathcal{S}^2$, the sum of the indexes of the fixed points in the interior of the surface of section must be either 1 or 3. In the first case, the periodic orbit represented by the border of

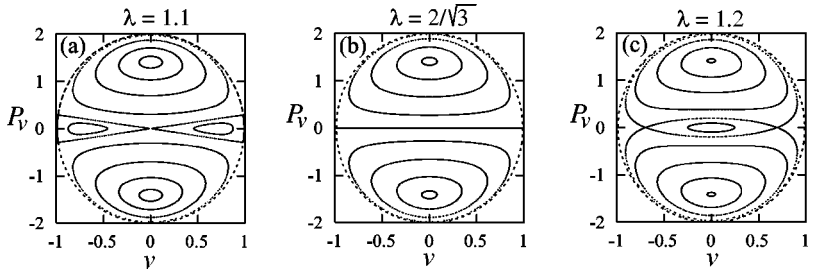

FIG. 8. Evolution of the surfaces of section $(u=0, P_u \geqslant 0)$ as a function of λ for $\epsilon = -2$ and $P_\phi = 0$. A third oyster bifurcation is observed between (a) and (c).

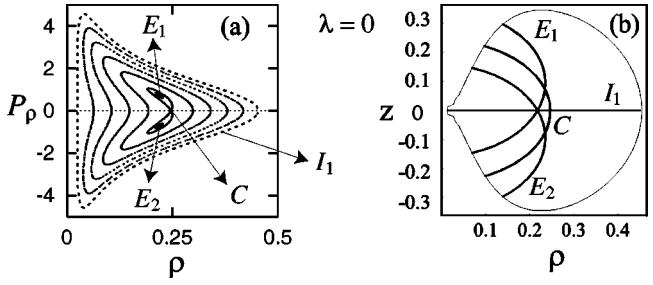

FIG. 9. (a) Surface of section ($z=0, P_z \geqslant 0$) for $\lambda=0$, $\epsilon=-2$ and $P_\phi=0.2$. (b) Periodic orbits.

the surface of section must be stable (index 1), while in the second one it must be unstable (index -1). In the case that the limit does not correspond to any periodic orbit, the sum of the indexes of the fixed points in the interior of the surface of section is always 2.

Let us now continue with the study of the evolution of the surface of section as the parameter λ increases. A first change—bifurcation—occurs when the value $\lambda=\sqrt{2}/3$ is reached (see Fig. 5): the two separatrix loops passing through the fixed points C merge with each other, in such a way that a degenerate curve of fixed points appears just for $\lambda=\sqrt{2}/3$. This curve, as can be checked by substituting $\lambda=\sqrt{2}/3$ into Eq. (24), corresponds to a circle of radius $\sqrt{2}$ when the scaled energy $\epsilon\rightarrow-\infty$. After this bifurcation, the degenerate set of equilibria disappears and the two pairs of fixed points I_∞ and C are created again with interchanged stability [see Fig. 5(c)]. In the literature, this bifurcation is called the as *oyster* bifurcation [28]. As a consequence of this bifurcation, while the quasiperiodic orbits around I_∞ disappear, a different kind of quasiperiodic orbit corresponding to the levels around C appears. These orbits always have the same symmetry pattern as C, that is to say, they are mainly localized around C.

As the parameter λ increases, a second *oyster* bifurcation takes place. Indeed, the separatrix loop enclosing the elliptic point I_1 shrinks [see Fig. 6(a)] in such a way that when $\lambda=\sqrt{2/3}$ the separatrix loop becomes a degenerate straight line of fixed points at the P_v axis [see Fig. 6(b)]. This set of fixed points corresponds to the rectilinear orbits $v=au$. When $\lambda>\sqrt{2/3}$, the fixed points I_1 and I_∞ appear again with interchanged stability [see Fig. 6(c)]. Moreover, as can be observed clearly in Fig. 6(d), the separatrix passing through I_1' degenerates at the limit of the surface of section because the periodic orbit I_1' is now unstable. As a consequence of this bifurcation, the levels—quasiperiodic orbits—around I_1' disappear, while the quasiperiodic orbits around I_∞ appear again.

In this second oyster bifurcation the periodic orbit I_1', which is at the limit of the section, suffers a stability change. For $\lambda<\sqrt{2/3}$, as the index of the section is 1, I_1' is a stable periodic orbit, whereas for $\lambda>\sqrt{2/3}$, as the index of the section is 3, I_1' becomes unstable [see Figs. 6(a) and 6(c)]. This stability change of orbit I_1' can be much better observed on the sphere $\mathcal{S}^2$. Figure 7 shows the evolution of $\mathcal{S}^2$ for the same λ values as in Fig. 6. In Fig. 7 can be seen the transformation of the periodic orbit I_1' from an elliptic fixed point into a hyperbolic fixed point [see Figs. 7(a) and 7(c)]. For $\lambda=\sqrt{2/3}$, the separatrices collapse in a degenerate meridian of fixed points [see Fig. 7(b)].

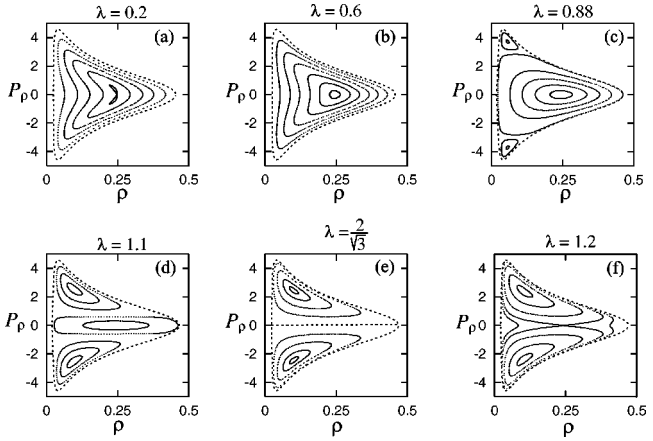

FIG. 10. Surfaces of section ($z=0, P_z \geqslant 0$) for $\lambda=0$, $\epsilon=-2$, and $P_\phi=0.2$.

Finally, a third oyster bifurcation (see Fig. 8) takes place when $\lambda>\sqrt{2/3}$. The separatrix lobe enclosing the fixed points I_∞ shrinks in such a way that when $\lambda=2/\sqrt{3}$ a degenerate line of fixed points appears on the v axis. When $\lambda>2/\sqrt{3}$, the degenerate set of equilibria disappears and the fixed points I_1 and C are created, in such a way that the phase space recovers the same structure as before the first bifurcation. For $\lambda>2/\sqrt{3}$ the structure of the surface of section does not suffer any further significant change.

It is worth noting that at three integrable limits the system shows high degeneracy. This situation has also been noted by Farrelly and Uzer [12] and by Elipe and Ferrer [28].

B. Case ($P_\phi \neq 0$)

In this case, there is no need to perform any kind of regularization for the Hamiltonian (4) because it does not present any singularity at $\boldsymbol{r}\rightarrow\boldsymbol{0}$.

First, we identify the values of the parameters (λ, P_ϕ) for which periodic analytical solutions exits. The Hamilton equations of motion arising from Eq. (4) are

$$\dot{\rho}=P_\rho, \quad \dot{P}_\rho=\frac{P_\phi^2}{\rho^3}-\left(1-\frac{\lambda^2}{2}\right)\rho-\frac{\rho}{(\rho^2+z^2)^{3/2}},$$

$$\dot{z}=P_z, \quad \dot{P}_z=-(\lambda^2 z)-\frac{z}{(\rho^2+z^2)^{3/2}}. \tag{29}$$

At first glance, we detect a family of rectilinear equatorial orbits along the ρ axis ($z=P_z=0$). These orbits, named I_1, exist always for all value of λ. At this point, we generate surfaces of section in the variables (ρ, z, P_ρ, P_z) by means of numerical integration of the equations of motion (29). The surface of section has been defined on the $z=0$ plane with $P_z \geqslant 0$. Thus, the available region for the system on this surface of section is bounded by the curves

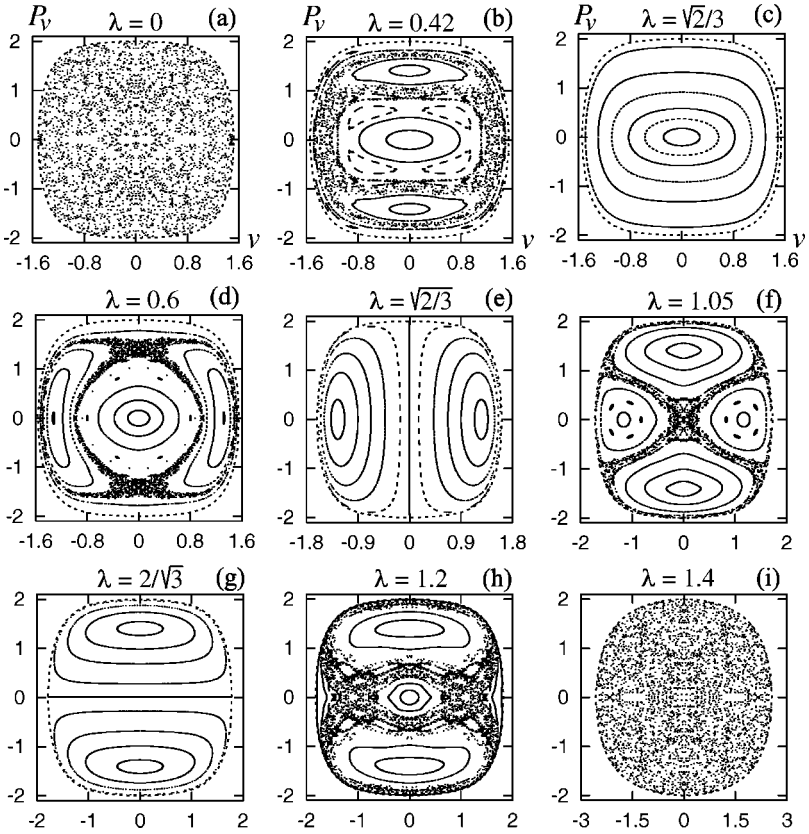

FIG. 11. Evolution of the surfaces of section ($u=0, P_u \geq 0$) for $\epsilon=-0.2$ as a function of λ in the case $P_\phi=0$.

$$P_\rho = \pm \sqrt{2\epsilon - \frac{P_\phi^2}{\rho^2} + \frac{2}{\rho} - \left(1 - \frac{\lambda^2}{2}\right)\rho^2}. \qquad (30)$$

It is important to note that these curves correspond to the rectilinear equatorial orbits I_1.

We keep constant the energy $\epsilon=-2$. In accordance with several numerical and perturbative studies [29], the phase space of the quadratic Zeeman case ($\lambda=0$) presents two different structures depending on whether P_ϕ is bigger or smaller than $1/\sqrt{-10\epsilon}$, and the transition from one to another takes place through a *pitchfork* bifurcation. In this way, we begin the study of the phase space evolution by fixing $P_\phi=0.2<1/\sqrt{20}$, while varying λ from 0 to $\sqrt{2}$.

When the quadratic Zeeman effect ($\lambda=0$) is considered, the corresponding surface of section reflects three periodic orbits corresponding to a hyperbolic fixed point and two elliptic fixed points [see Fig. 9(a)]. These periodic orbits, called, respectively, E_1, E_2, and C, are depicted in Fig. 9(b).

As in the case $P_\phi=0$, because the rectilinear equatorial orbit I_1 corresponds to the limit of the surface of section, its stability cannot be determined at a glance. However, its stability can be determined by applying the index theorem: because the index of the surface of section is 1 (there are two stable fixed points and one unstable), the periodic orbit I_1 is necessarily stable.

When the parameter λ is turned on, the separatrix lobes shrink; compare Fig. 9(a) to Fig. 10(a) for $\lambda=0.2$. The two stable fixed points $E_{1,2}$ and the unstable one C come into coincidence when $\lambda \approx 0.246\,183$ in such a way that only I_1 survives, becoming stable [Fig. 10(b)]; a pitchfork bifurcation takes place.

As λ increases, two other stable fixed points (periodic orbits) appear in the lower and upper corners of the limit of the surface of section [see Fig. 10(c)]. We call these equilibria $E'_{1,2}$. The appearance of these structures brings a change in the index of the surface of section, which is now 3. Hence, the periodic orbits I_1 become unstable. In other words, an additional pitchfork bifurcation has occurred.

A final change in the phase space structure is detected when λ increases. The separatrix lobes enclosing the fixed points $E'_{1,2}$ grow as λ approaches $2/\sqrt{3}$ [Fig. 10(d)], in such a way that they merge along the $P_\rho=0$ axis when $\lambda=2/\sqrt{3}$, an integrable case. As a consequence, the ρ axis becomes a degenerate straight line of fixed points [Fig.

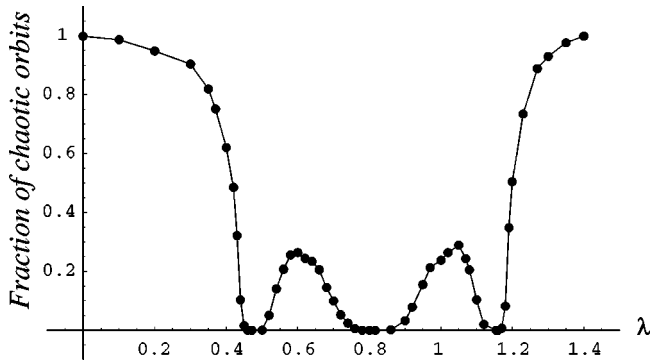

FIG. 12. Evolution of the fraction of chaotic orbits in the surface of section as a function of λ for $P_\phi=0$ and $\epsilon=-0.2$.

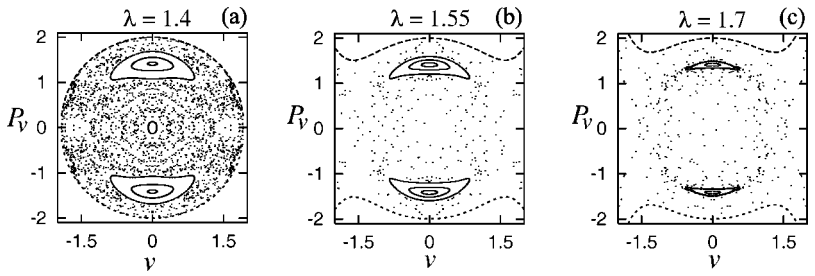

FIG. 13. Evolution of the surfaces of section ($u=0, P_u \geq 0$) for $\epsilon=-0.5$ as a function of λ in the case $P_\phi=0$.

10(e)]. When $\lambda > 2/\sqrt{3}$, from this degenerate straight line again the hyperbolic point C is created [see Fig. 10(f)]. This change can be explained in terms of an oyster bifurcation, and somehow we recover a similar situation to the one we had before the first pitchfork bifurcation. For $\lambda > 2/\sqrt{3}$, the phase space structure does not suffer any more significant change.

V. CHAOTIC BEHAVIOR AND IONIZATION DYNAMICS

In the previous sections, we studied the evolution of the structure of the phase space of the complete system, making use of surfaces of section. All these surfaces of section were computed for $\epsilon=-2$. For this energy value, the phase space exhibits a global regular structure: all orbits are regular and confined to adiabatic invariant tori. The reason that all the Poincaré surfaces calculated in the previous section are so regular is that, for the range of values $0 \leqslant \lambda < \sqrt{2}$ that we have considered, the effective potential has no saddle point—the electron cannot ionize—and thus the value $\epsilon=-2$ is small enough to consider the system as an infinitesimally perturbed hydrogen atom.

At this point, it is important to study the system behavior when its energy is much bigger. Hence, in this section, we analyze the effect of the parameter λ on the dynamics of our system when the scaled energy ϵ takes a fixed small negative value. In particular, we focus on the case $P_\phi=0$. Figure 11 shows a gallery of surfaces of section for $\epsilon=-0.2$ and increasing values of λ.

The sequence begins with $\lambda=0$ [Fig. 11(a)], the well-known quadratic Zeeman effect. As can be seen, global chaos completely dominates the dynamics of the system. As λ varies between $0<\lambda \leqslant 1.4$, we observe three chaos-order-chaos transitions. As λ approaches each of the three integrable limits $\lambda_i=(\sqrt{2}/3, \sqrt{2/3}, 2/\sqrt{3})$, the stochastic motion gradually disappears in such a way that at the corresponding integrable λ_i value the expected regularity is reached. On the other hand, when λ moves away from each integrable value, the regions of stochastic motion grow in size. In particular, for $\lambda=1.4$ [Fig. 11(i)] the dynamics of the system is totally dominated by chaotic motion.

A clear way to illustrate the order-chaos transitions showed in Fig. 11 is to measure the fraction of the phase space where the trajectories are chaotic. To do this, for $\epsilon=-0.2$ and a given λ value, we have numerically calculated the maximum Lyapunov exponent [30] of a large number of orbits with initial conditions arranged on a fine grid that covers the corresponding surface of section. In this way, we have been able to measure numerically, for each value of λ, the fraction of the area of the surface of section covered by chaotic trajectories.

In Fig. 12 we show the result of this procedure for $0 \leqslant \lambda \leqslant 1.4$ and $\epsilon=-0.2$. This figure confirms the features of the three consecutive chaos-order-chaos transitions observed in the sequence of surfaces of section shown in Fig. 11.

An interesting question appears when the ionization dynamics is considered, e.g., when $\lambda > \sqrt{2}$. We have just noted that for $\lambda=1.4$ and $\epsilon=-0.2$, the phase space is filled with chaotic orbits. Hence, when λ is further increased, and the threshold ionization energy E_2 becomes smaller than $\epsilon=-0.2$, all trajectories have access to the ionization channel located along the ρ axis. However, for smaller values of ϵ, the ionization mechanics is different. This fact can be observed in the surfaces of section shown in Fig. 13 for $\epsilon=-0.5$. In Fig. 13(a) for $\lambda=1.4$, some regular orbits are isolated from the chaotic region by KAM tori located around the periodic orbits I_∞ and I_1. When λ increases and the ionization energy is below -0.5 [Figs. 13(b) and (c)], the islands around I_∞ survive, in such way that the orbits inside them remain confined. All orbits outside these tori ionize, and this is why the area between the islands is empty. Note that in Fig. 13(b) and Fig. 13(c) the surface of section is not a bounded region because the rectilinear orbit I_1'—which corresponds to the limit of the surface of section—escapes through the ionization channel.

In fact, I_1 and I_1' are the first orbits that have access to the ionization channel because they are rectilinear orbits along the ρ axis. On the contrary, the islands around the periodic orbits I_∞ survive because the orbits inside remain isolated from this channel.

We can explain the different ionization behavior found for $\epsilon=-0.2$ and $\epsilon=-0.5$ by calculating for these energies the evolution of the (maximum) Lyapunov exponent of I_∞ and I_1 as a function of λ. For $\epsilon=-0.2$, this evolution is shown in Fig. 14(a). We observe in this figure that, before the threshold energy is reached for $\lambda \approx 1.415\,89$, both periodic orbits become chaotic, which explains why the surface of section for $\lambda=1.4$ is filled with chaotic orbits. For $\epsilon=-0.5$ [see Fig. 14(b)], while the Lyapunov exponent of I_1 shows a similar behavior as in the case $\epsilon=-0.2$, the periodic orbit I_∞ remains regular for energies bigger than the ionization energy for $\lambda \approx 1.440\,16$. Hence, two islands of regular orbits around I_∞ persist, as shown in Fig. 13(b) and Fig. 13(c).

Finally, because the ionization dynamics depends on the energy ϵ, this could lead to different ionization probabilities because, for a given λ value, the ionization threshold is the same. A similar behavior was observed by Uzer and Farrelly

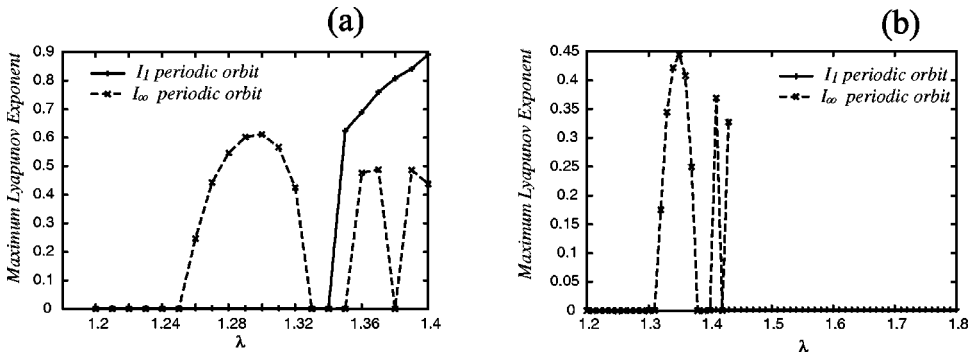

FIG. 14. Lyapunov exponent of the periodic orbits I_∞ and I_1 as a function of λ. (a) $\epsilon=-0.2$. (b) $\epsilon=-0.5$.

in the hydrogen atom in crossed electric and magnetic fields [31].

VI. CONCLUSIONS

We investigate the classical dynamics of a hydrogen atom in the presence of uniform magnetic and quadrupolar electric fields. Owing to the axial symmetry, the z component of the canonical angular momentum P_ϕ is conserved, and hence the system, expressed in cylindrical coordinates, has two degrees of freedom. After scaling coordinates and momenta in the usual form, the Hamiltonian depends only on two parameters. On the one hand, it depends on P_ϕ; and on the other, it also depends on a dimensionless parameter λ that represents the relative field strengths. We note that when $\lambda<\sqrt{2}$ this Hamiltonian is equivalent to the Hamiltonian of the generalized van der Waals interaction. The shape of the effective potential surface and its critical points are studied depending on the system parameters. This study shows that when $\lambda<\sqrt{2}$ the atom, even for positive energies, cannot ionize. However, for $\lambda>\sqrt{2}$ the electron has the possibility of escaping along the channel created by a saddle point located at the ρ axis. We find that the three integrable cases $\beta=(\pm 1/2,\pm 1,\pm 2)$ of the generalized van der Waals problem appear in our system for $\lambda=(\pm\sqrt{2}/3,\pm\sqrt{2/3},\pm 2/\sqrt{3})$, respectively. In this sense, we have determined the three corresponding integrals of motion. We note that, while the integrals of motion corresponding to $\lambda=\pm\sqrt{2/3}$ and $\beta=\pm 1$ are the same, the integrals of motion for $\lambda=(\pm\sqrt{2}/3,\pm 2/\sqrt{3})$ are neither equal nor equivalent to the integrals for $\beta=(\pm 1/2,\pm 2)$. For $\lambda=\pm\sqrt{2/3}$ and $\lambda=\pm 2/\sqrt{3}$ the Hamiltonian is separable in spherical and semiparabolic coordinates, respectively, while for $\lambda=\pm\sqrt{2}/3$ we have not been able to find any coordinate system as a function of which the Hamiltonian is separable. By means of Poincaré surfaces of section, the phase space evolution in the regular regime is studied as a function of the parameters P_ϕ and λ. We study separately the cases $P_\phi=0$ and $P_\phi\neq 0$. For $P_\phi=0$, we find that the system suffers three consecutive oyster bifurcations at the integrable values $\lambda=(\pm\sqrt{2}/3,\pm\sqrt{2/3},\pm 2/\sqrt{3})$. In order to better visualize these bifurcations, we have introduced a transformation that maps the surface of section onto a two-dimensional sphere. For $P_\phi=0.2$ we detect another three bifurcations; two of them are pitchfork bifurcations, while the other is an oyster bifurcation at the integrable value $\lambda=\pm 2/\sqrt{3}$. The chaotic behavior of the system is studied and three order-chaos transitions are found when the system passes through the integrable cases. Finally, we find two different behaviors in the ionization mechanics. In both cases, the ionization is explained in terms of the stability of the periodic orbits I_1 and I_∞.

To conclude, as we remark in the Introduction, while the generalized van der Waals problem has a real physical counterpart only for certain values of the parameters, we recall that our problem always corresponds to a real physical system that may be experimentally implemented.

ACKNOWLEDGMENT

This research has been partially supported by the Spanish Ministry of Education (DGES Project Nos. PB98-1576 and BFM2002-03157).

[1] H. Friedrich and D. Wintgen, Phys. Rep. **183**, 37 (1989); J. Main and G. Wunner, Phys. Rev. Lett. **82**, 3038 (1999).

[2] J. Gao and J. B. Delos, Phys. Rev. A **49**, 869 (1994); M. Courtney, H. Jiao, N. Spellmeyer, D. Kleppner, J. Gao, and J. B. Delos, Phys. Rev. Lett. **74**, 1538 (1995).

[3] P. M. Koch and K. A. H. van Leewen, Phys. Rep. **255**, 290 (1995).

[4] T. Uzer, D. Farrelly, J. Z. Milligan, P. E. Raines, and J. P. Skelton, Science **242**, 42 (1991); J.-M. Mao, K. A. Rapelje, S. J. Blodgett-Ford, J. B. Delos, A. König, and H. Rinneberg, Phys. Rev. A **48**, 2117 (1993); A. D. Peters, C. Jaffé, and J. B. Delos, Phys. Rev. Lett. **73**, 2825 (1994).

[5] G. Wiebusch, J. Main, K. Krüger, H. Rottke, A. Holle, and K. H. Welge, Phys. Rev. Lett. **62**, 2821 (1989); G. Raithel, M. Fauth, and H. Walther, Phys. Rev. A **44**, 1898 (1991); **47**, 419 (1993); A. D. Peters and J. B. Delos, *ibid.* **47**, 3020 (1993); **47**, 3036 (1993); C. Neumann, R. Ubert, S. Freund, E. Flöthmann, B. Sheehy, K. H. Welge, M. R. Haggerty, and J. B. Delos, Phys. Rev. Lett. **78**, 4705 (1997).

[6] P. Schmelcher and W. Schweizer, *Atoms and Molecules in*

Strong External Fields (Plenum Press, New York, 1998); H. Hasegawa, M. Robnik, and G. Wunner, Prog. Theor. Phys. Suppl. **98**, 198 (1989).
[7] Y. Alhassid, E. A. Hinds, and D. Meschede, Phys. Rev. Lett. **59**, 1545 (1987).
[8] J. E. Lennard-Jones, Trans. Faraday Soc. **28**, 334 (1932).
[9] K. Ganesan and M. Lakshmanan, Phys. Rev. Lett. **62**, 232 (1989).
[10] K. Ganesan and M. Lakshmanan, Phys. Rev. A **42**, 3940 (1990).
[11] J. E. Howard and D. Farrelly, Phys. Lett. A **178**, 62 (1993); D. Farrelly and J. E. Howard, Phys. Rev. A **48**, 851 (1993).
[12] D. Farrelly and T. Uzer, Celest. Mech. Dyn. Astron. **61**, 71 (1995).
[13] W. Paul, Rev. Mod. Phys. **62**, 531 (1990).
[14] R. Blümel, C. Kappler, W. Quint, and H. Walther, Phys. Rev. A **40**, 808 (1989).
[15] K. Ganesan and M. Lakshmanan, Phys. Rev. A **45**, 1548 (1992).
[16] K. Ganesan and M. Lakshmanan, Phys. Rev. A **48**, 964 (1993).
[17] M. W. Beims and J. A. C. Gallas, Phys. Rev. A **62**, 043410(12) (2000).
[18] R. Blümel and W. P. Reinhardt, *Chaos in Atomic Physics*, Cambridge Monographs on Atomic, Molecular and Chemical Physics Vol. 10 (Cambridge University Press, Cambridge, England, 1997), pp. 290–293.
[19] F. M. Penning, Physica (Amsterdam) **3**, 873 (1936); H. Dehmelt, Rev. Mod. Phys. **62**, 525 (1992).
[20] G. Zs. K. Horvath, J. L. Hernandez-Pozos, K. Dholakia, J. Rink, D. M. Segal, and R. C. Thompson, Phys. Rev. A **57**, 1944 (1998).
[21] J. Stoer and R. Bulirsch, *Introduction to Numerical Analysis* (Springer-Verlag, New York, 1983).
[22] J. P. Salas, A. Deprit, S. Ferrer, V. Lanchares, and J. Palacián, Phys. Lett. A **242**, 83 (1998).
[23] T. Levi-Civitá, *Sur la Resolution Qualitative du Probléme des Trois Corps* (University of Bologna Press, Bologna, 1956), Vol. 2.
[24] M. C. Gutzwiller, *Chaos in Classical and Quantum Mechanics* (Springer-Verlag, Berlin, 1990).
[25] J. D. Lambert, *Computational Methods in Ordinary Differential Equations* (John Willey & Sons, London, 1976).
[26] W. S. Massey, *Algebraic Topology: An Introduction* (Springer-Verlag, Berlin, 1987).
[27] V. I. Arnol'd, *Ordinary Differential Equations* (Springer-Verlag, New York, 1992).
[28] A. Elipe and S. Ferrer, Phys. Rev. Lett. **72**, 985 (1994).
[29] A. Deprit, V. Lanchares, M. Iñarrea, J. P. Salas, and J. D. Sierra, Phys. Rev. A **54**, 3885 (1996).
[30] A. Wolf, J. B. Swift, L. Swinney, and J. A. Vastano, Physica D **16**, 285 (1985).
[31] T. Uzer and D. Farrelly, Phys. Rev. A **52**, R2501 (1995).